Experimental and Numerical Study of the Mechanical Behaviour of an Unfilled Silicone Rubber

Luc Meunier, Grégory Chagnon, Denis Favier, Laurent Orgéas

Experimental and Numerical Study of the Mechanical Behaviour of an Unfilled Silicone Rubber

L. Meunier, G. Chagnon, D. Favier & L. Orgéas
Laboratoire Sols-Solides-Structures (3S), CNRS – Universités de Grenoble (UJF-INPG) , BP 53 , 38041 Grenoble cedex 9, France

ABSTRACT: In this contribution, the mechanical behaviour of an unfilled silicone rubber was analysed. Firstly, tensile and pure shear tests were carried out on silicone plates. During the tests, full-field measurements of the strain on the surface of deformed samples were obtained using a Digital Image Correlation technique. Results show that Mullins effects, hysteresis as well as strain rate sensitivity can be considered as negligible. Consequently, three hyperelastic models were fitted with the experimental data (Mooney, Gent and Haines & Wilson models). Secondly, a plate silicone sample containing holes was deformed in tension. In parallel, Finite Element simulation of this experiment was performed with the fitted hyperelastic models. The comparison of experimental and numerical results emphasizes the importance of the choice of the hyperelastic modelling in the simulation of strain fields. For example, this could be fundamental for crack tip analysis.

1 INTRODUCTION

Owing to their good biocompatibility properties, silicone rubbers are being increasingly used in biomedical applications. Unfortunately, experimental studies aimed at analysing and modelling the mechanical behaviour of such materials are quite scarce (Podnos et al. 2006, Loew & Meier 2006, Goulbourne et al. 2007). This is a lack for the development of structural applications involving silicone rubber parts. Within that context, and towards a better understanding of the mechanics of silicone rubbers, we have processed plates using an unfilled silicone rubber formulation (section 2). The plates have then been deformed using homogeneous tensile and pure shear deformation tests. During the tests the local strain field on the surface of deformed samples was obtained using a visible CCD camera and a Digital Image Correlation technique (section 3). Experimental results are given in section 4 and prove that Mullins effects, hysteresis as well as strain rate sensitivity are weak. This permits to model the mechanical behaviour of the studied silicone with hyperelastic formalism. Three hyperelastic models are fitted with the experiments, *i.e.* Mooney (1949), Gent (1996) as well as Haines & Wilson (1979) models. Lastly, in order to test the capability of the above constitutive schemes to model the deformation of complex structures, (i) a plate silicone sample containing holes is deformed in tension, (ii) Finite Element simulation of this experiment is performed with the three fitted hyperelastic models, and (iii) a comparison of resulting experimental and numerical local strain fields is achieved (section 5).

2 MECHANICAL TESTING PROCEDURE

The chosen silicone rubber is a unfilled formulation produced by Rhodia (RTV 141). Thin plates with an approximate thickness of 2 mm and in-plane dimensions 180×100 mm² were produced using the following processing route: (i) mixing the two liquid components with a 1/10 ratio (ii) filling the rectangular mould with the liquid mixture, (iii) putting the mould with the uncured mixture under vacuum for 10 min in order to eliminate undesirable entrapped bubbles, (iv) putting the mould inside a oven at 70°C for 150 min to cure the silicone. Thereafter, the upper faces of the plates were coated with a random pattern made of small speckles (red silicone). Lastly, specimens were cut from the plates using specially designed hollow punches. Notice that a particular attention was paid to respect such a procedure, in order to obtain specimens with reproducible mechanical properties. Also notice that the quality of the coated pattern is decisive to gain a good estimation of the local strain field (see next section).

3 MECHANICAL TESTING PROCEDURE

All the tested samples were deformed using an universal mechanical tensile testing machine (MTS

4M), using both an axial load cell of 125 daN and specially designed autoblocking grips (Fig. 1). During the tests, the deformation of samples and their superimposed pattern was recorded using a CCD camera (JAI, 1280×1024 pixels, 25Hz, see figure 1). Using the Digital Image Correlation Software 7D (Vacher 2003), it was then possible to determine the local strain field on the surface of the deformed samples.

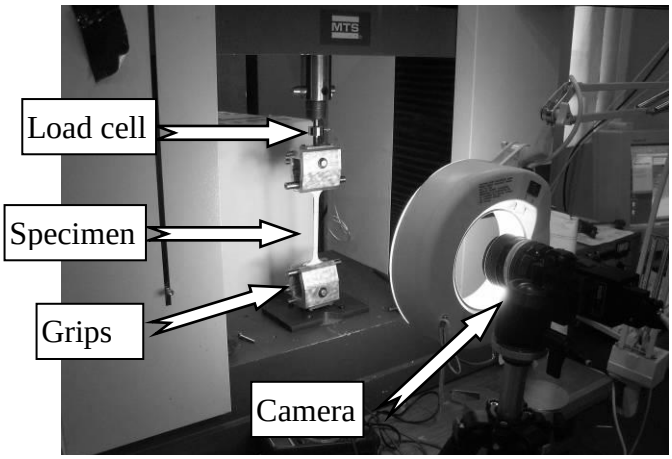

Figure 1. Testing machine with tensile test specimen and CCD camera

In order to analyse the mechanical behaviour of the silicone, samples were subjected to two types of homogeneous loadings and one heterogeneous one:

- Simple tensile tests were performed on bone samples having an initial gauge length l_0 of 60 mm and a gauge cross section S_0 of 12×2 mm² (Fig. 2(a)).
- Pure shear strain state was approached by performing plane strain tensile tests (Fig. 2(b)). The height l_0 as well as the width b_0 of samples were 6 mm and 70 mm, respectively.
- A tensile test was also performed on a plate (height $l_0 = 80$ mm, width $b_0 = 70$ mm) containing five holes (Fig. 3). The central hole has a diameter of 24 mm, whereas the four other hole's diameter was set to 19 mm. Notice that the positions of the centres have not been positioned to produce a regular arrangement, so that the plate does not have any symmetry.

For the two homogeneous tests, monotonic as well as cyclic loadings were performed at constant elongation rate $\dot{l} / l_0$ ranging from $2\ 10^{-4}\ s^{-1}$ to $10^{-1} s^{-1}$ (l being the current gauge length). The analysis of the local displacement field deduced from 7D also proved that the strain state in the gauge zones could fairly be considered as homogeneous. Moreover, the plate with holes was subjected to a monotonic loading at a constant crosshead velocity $\dot{l} = 2\ 10^{-4}$ mm s^{-1}. For this test, strong strain heterogeneities were recorded.

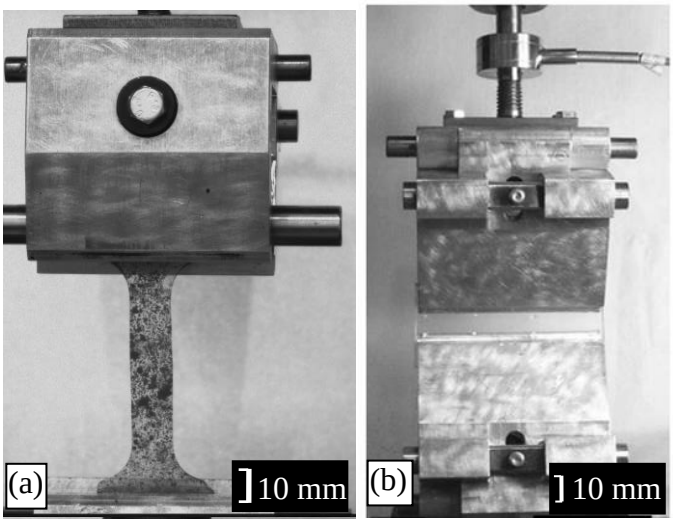

Figure 2. (a) Simple tensile test specimen and (b) pure

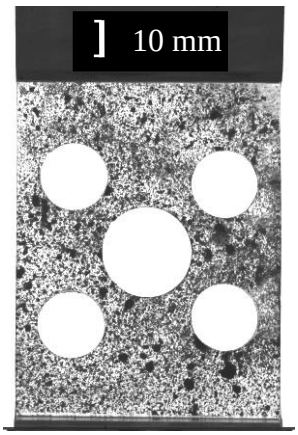

Figure 3. Plate with five holes

4 HOMOGENEOUS TEST

4.1 *Tests and results*

Experiments were designed to evaluate different physical aspects of rubber materials. First, a cyclic tensile test has been performed. Two cycles are realized at six increasing stress levels (cf. timing diagram of figure 4) at 0.008 s^{-1} elongation rate. This test was designed to evaluate the Mullins effect and hysteretic behaviour of the silicone.

The curves of figure 4 show a perfect non linear elastic behaviour without Mullins effect or hysteretic behaviour since all loading and unloading curves are superimposed.

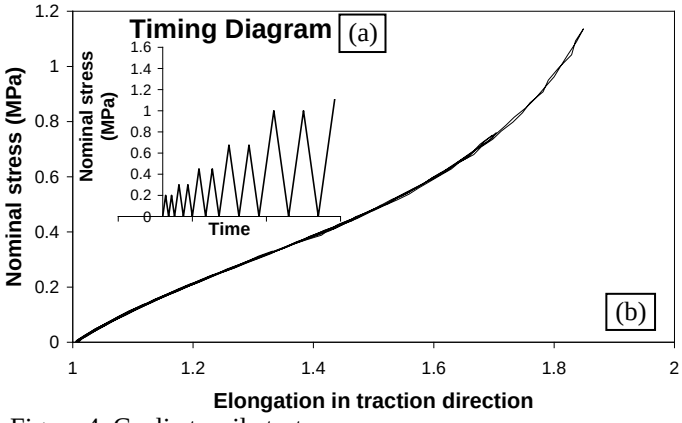

Figure 4. Cyclic tensile test:
(a) timing diagram of the load applied $\dot{l} / l_0 = 0.008\ s^{-1}$
(b) nominal stress – elongation behaviour

Furthermore, the strain rate sensitivity of this silicone has been studied through a two cycles test at different strain rates: 2 10^{-4} s^{-1} and 10^{-1} s^{-1}. A single specimen has been subjected to two cycles, one at each strain rate. Figure 5 shows no noticeable difference between the cycles so that we can assume the behaviour does not depend on the strain rate within the considered range.

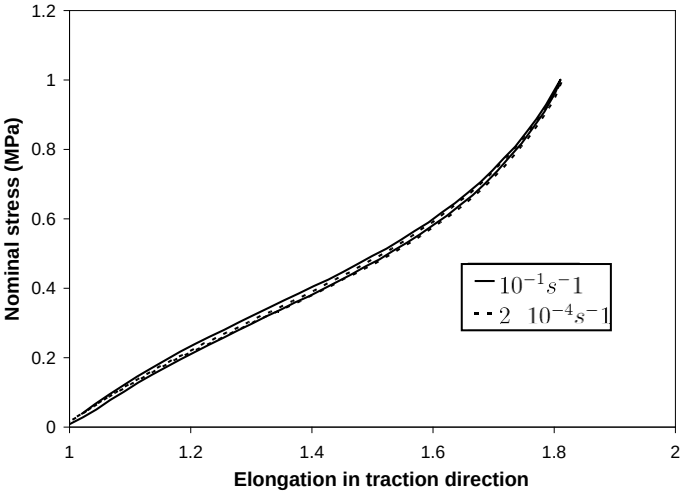

Figure 5. Cyclic tensile test at two different strain rates

Last, a relaxation test has been performed to test the time dependency of the silicone rubber in a different way. The global force was measured on the bounds of a simple tensile specimen when blocking the elongation at 1.8 for 14 hours. During that time, the stress diminished by 3% (Fig. 6). Consequently it is concluded that the RTV 141 behaviour presents a non-linear elasticity with very few time dependence and without Mullins effect.

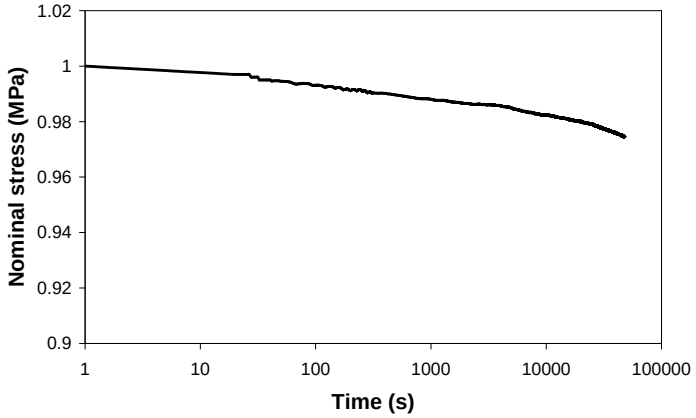

Figure 6. Relaxation test on a tensile test specimen at an elongation of 1.8

4.2 *Identification*

Considering the results given in the previous paragraph, a hyperelastic model seems perfectly adapted to represent the silicone's behaviour. Three energy densities have been chosen: Mooney (1940), Haines and Wilson (1979) and Gent (1996). They depend on the first and second invariants of the right Cauchy-Green tensor. Constitutive equations of the energy densities are presented in table 1. These models have been chosen because they are representative, but not exhaustive, of hyperelastic models. Mooney model is the most used in rubber industrial development. Haines and Wilson is a high order of Rivlin (1951) series whereas Gent model is representative of non-Gaussian hyperelastic laws (Boyce 1996).

Mooney	$W_M =$	$C_{10}(I_1-3)+C_{01}(I_2-3)$
Gent	$W_G =$	$-\frac{E}{6}(I_m-3)ln\left[1-\frac{I_1-3}{I_m-3}\right]$
Haines & Wilson	$W_{HW} =$	$C_{10}(I_1-3)+C_{20}(I_1-3)^2$ $+C_{30}(I_1-3)^3+C_{01}(I_2-3)$ $+C_{02}(I_2-3)^2+C_{11}(I_1-3)(I_2-3)$

Table 1. Hyperelastic energy density constitutive equations

The energy density parameters have been fitted on experimental data from tensile and pure shear tests. The values of the parameters are presented in table 2.

Mooney	$C_{10}=0.18$	$C_{01}=0.056$	
Gent	$E=1.23$	$I_m=7.2$	
Haines & Wilson	$C_{10}=0.23$	$C_{20}=-0.021$	$C_{30}=0.024$
	$C_{01}=0$	$C_{02}=0$	$C_{11}=-0.0033$

Table 2. Values of the hyperelastic energy parameters

Figures 7 and 8 present respectively a comparison between simulations using the hyperelastic energy densities and experimental data for tensile and pure shear tests.

Results given here show that the Mooney model can only describe the silicone rubber at low strains because it is unable to represent the strain hardening of the material. On the contrary, Gent and Haines & Wilson models have good results for the whole curves. Nevertheless, Haines and Wilson model is more difficult to fit because of the number of parameters.

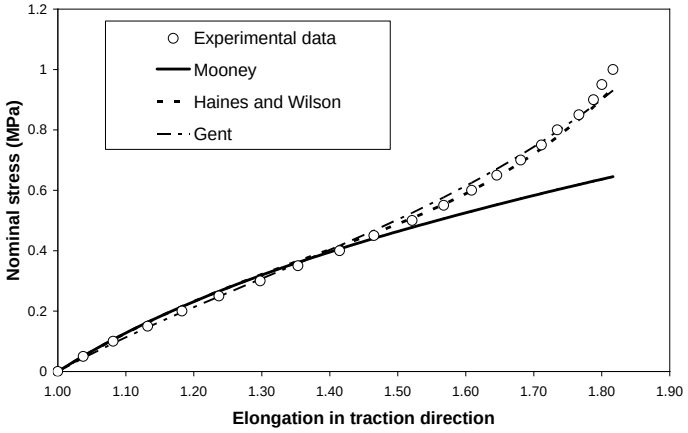

Figure 7. Simulation of a tensile test with the three hyperelastic models and comparison with experimental data

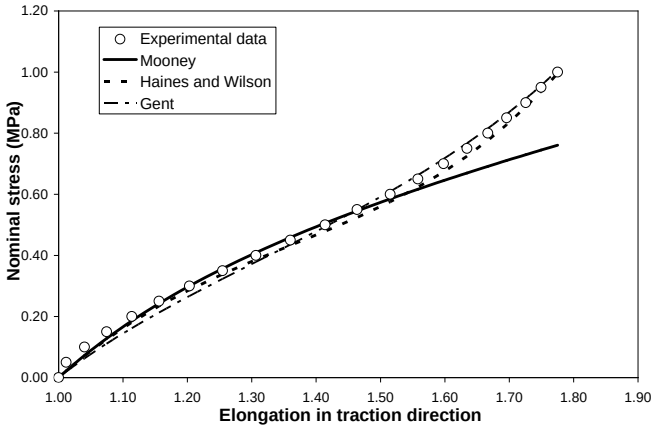

Figure 8. Simulation of a pure shear test with the three hyperelastic models and comparison with experimental data

5 HETEROGENEOUS TESTS

To validate the models fitted on uniaxial data, a test with heterogeneous strain fields has been used.

5.1 *Experimental results*

Figure 9 shows a representation of the major principal logarithmic strain field at an current force of 36N, i.e. below the failure of the plate. When increasing the force, a failure occurred between the central hole and the lower right hole. The deformation at a force of 40N, i.e. after the failure, is presented in figure 10.

Some voids are visible in figure 9a owing to local correlation problems in relation with too large speckles in the pattern.

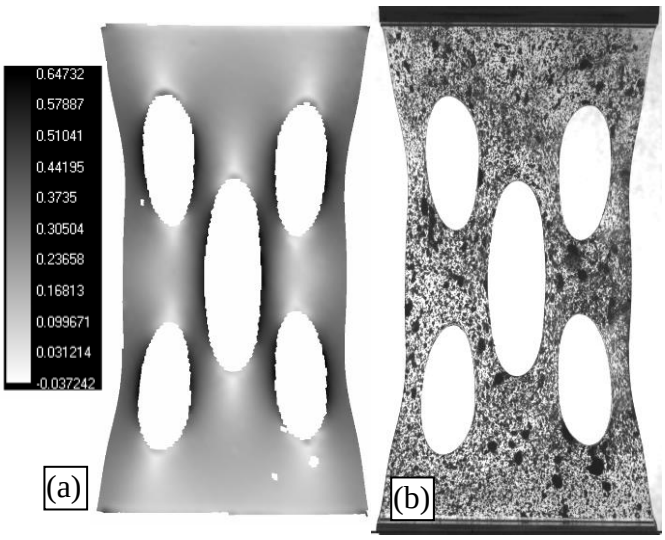

Figure 9. (a) Major principal logarithmic strain in the plate with holes submitted to 36N; (b) deformation of the pattern

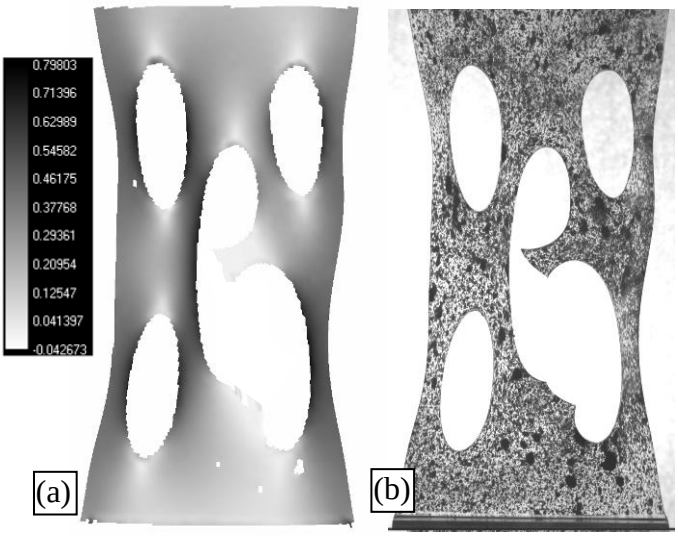

Figure 10. (a) Major principal logarithmic strain in the plate with holes submitted to 36N; (b) deformation of the pattern

5.2 *Numerical predictions*

The numerical simulations of the above experiment were performed with the finite element code ABAQUS. The material coefficients used are those presented in table 2. The Gent model needs an Umat subroutine while Mooney and Haines & Wilson models are already implemented in ABAQUS. For numerical convenience, the material's models were defined hardly compressible; elements quadratic in displacement and linear pressure were used (C4D20H, see figure 11).

The finite element model geometry was designed using the dimensions of the experimental plate data. It is a 3D model. Furthermore, the holes positions are not symmetric thereby the model could not be reduced.

The lower side of the model is fixed and the upper face has a rigid body vertical displacement and the global force is applied on this face. These boundary conditions are designed to fit the experiment conditions.

5.3 *Comparison*

This part presents results of the experiments and numerical simulations processed in such way that it is possible to compare the data. Three horizontal paths are used: one passing through the upper holes, one through the central hole and one through the lower holes (Fig. 11).

Both states at 36 N and 40N are considered. The test at 36 N has rather moderate strains while the test at 40 N, after partial breakage, induces higher strains.

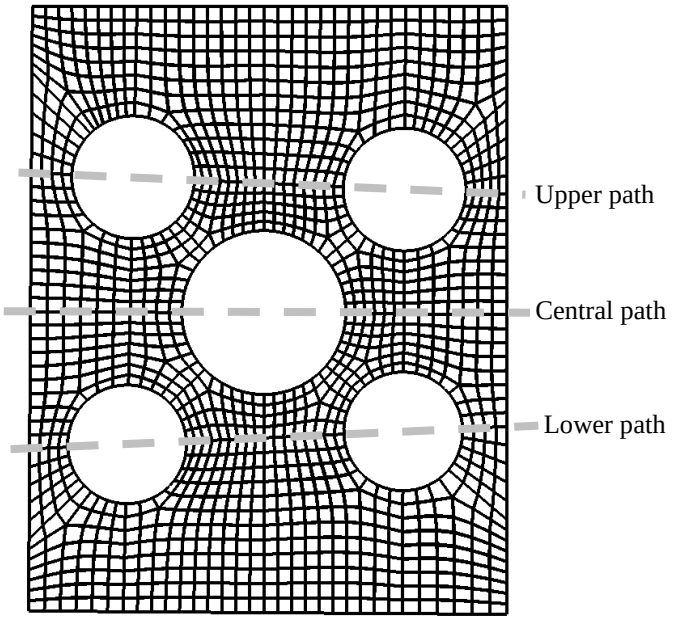

Figure 11. FE mesh and paths from which the strain data is extracted

5.3.1 *Below failure*

The strain fields considered here have been obtained experimentally through 7D correlation software and numerically with ABAQUS. For the 36N loading, the maximum principal elongation has been plotted along the upper and central paths described previously. The results are respectively presented in figures 12 and 13.

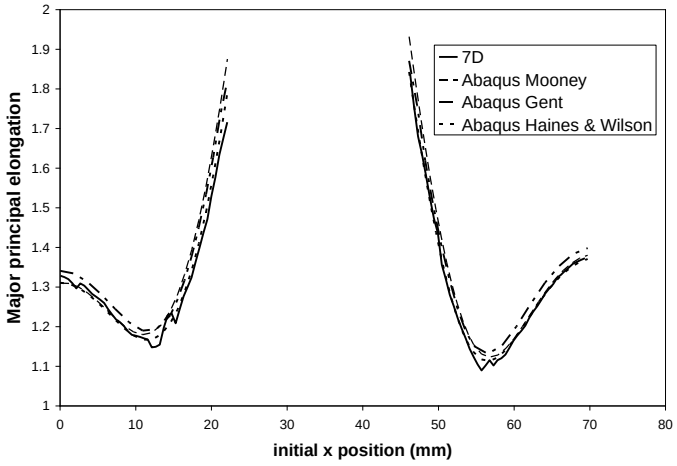

Figure 12. Experimental and simulated elongations along the central path at 36N

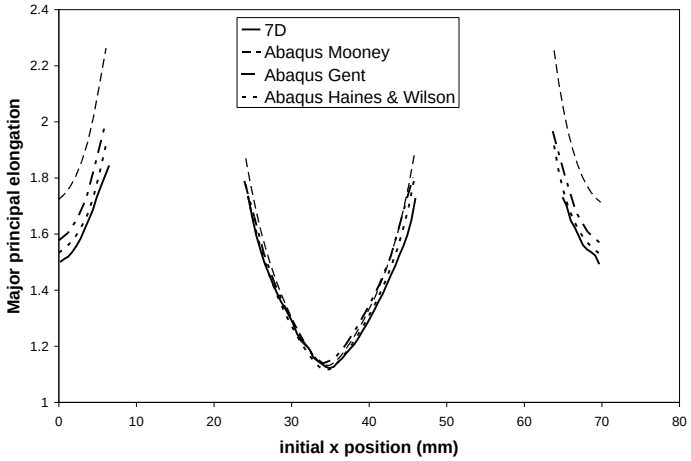

Figure 13. Experimental and simulated elongations along the upper path at 36N

Results show a good agreement between simulations and experiment for the central path (Fig. 12) but the strain remains at a moderate level. But for large deformation on the upper path (Fig. 13) Mooney constitutive equation gives strains too high especially where the elongation is high. It gives an error up to 40% of deformation whereas Gent and Haines & Wilson remain in good accordance with the experimental measurements.

5.3.2 *Above failure*

In that situation the geometry of the numerical models had to be modified to take into account the breakage. When applying a force of 40N, the differences between simulations and experiment are increased: the partial failure induced higher strain levels in the healthy parts of the plate.

Figure 14 shows a comparison between the photograph of the specimen and the shape predicted by the simulations. In the images, the black outlines are the FE models contour lines.

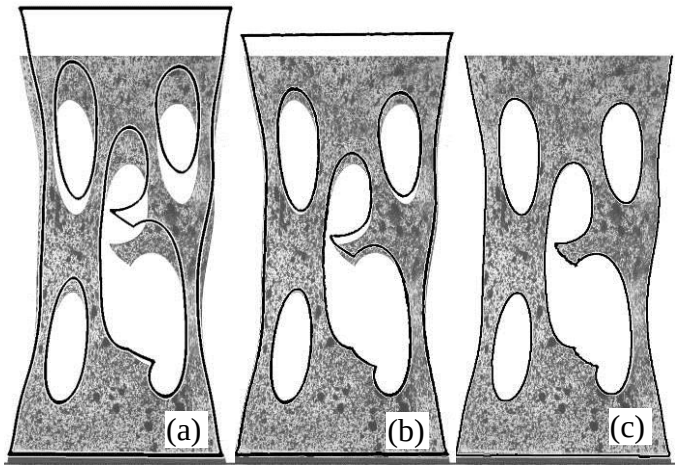

Figure 14. Comparison of global deformations predicted by the different constitutive models and the experimental data at 40N: (a) Mooney, (b) Gent and (c) Haines & Wilson

Once again, the model using Mooney constitutive equation predicts too large deformations while Gent and particularly Haines & Wilson are better.

The curves describing the major elongation are presented in figure 15 for the upper path, in figure 16 for the central path and in figure 17 for the lower path.

Mooney model gives good results for moderate strain while Gent and Haines & Wilson still well fit to the experimental data at large strains. Indeed Mooney model cannot describe the strain hardening of the material and becomes too soft for large deformations thus inducing important errors (120% on the right side of lower path, Fig. 17).

In this case, Gent is a little too soft but still has moderate errors i.e. 20% at the same place. Haines & Wilson gives very good results for every path and at all levels.

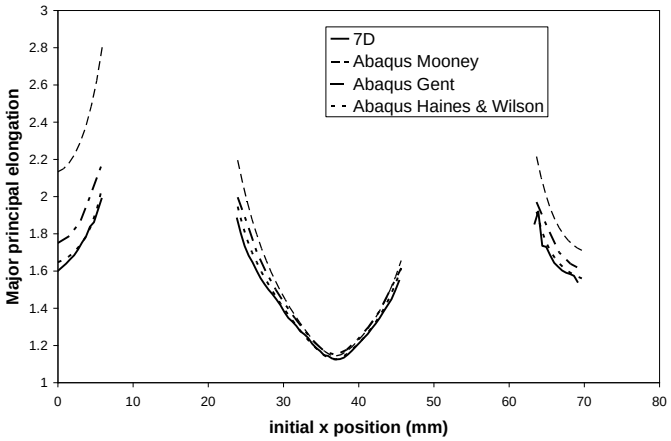

Figure 15. Experimental and simulated elongations along the upper path at 40N

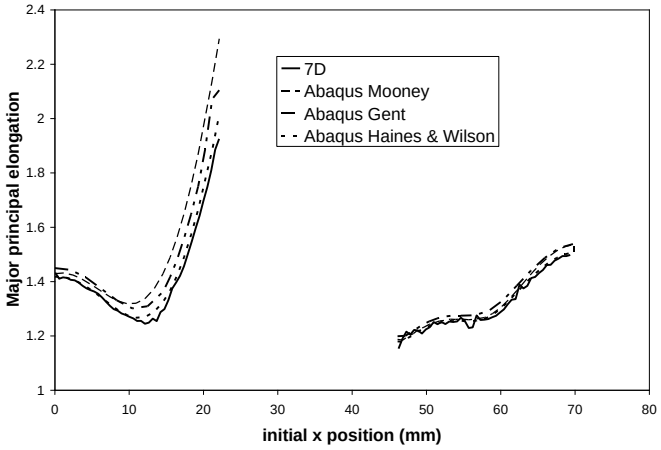

Figure 16. Experimental and simulated elongations along the central path at 40N

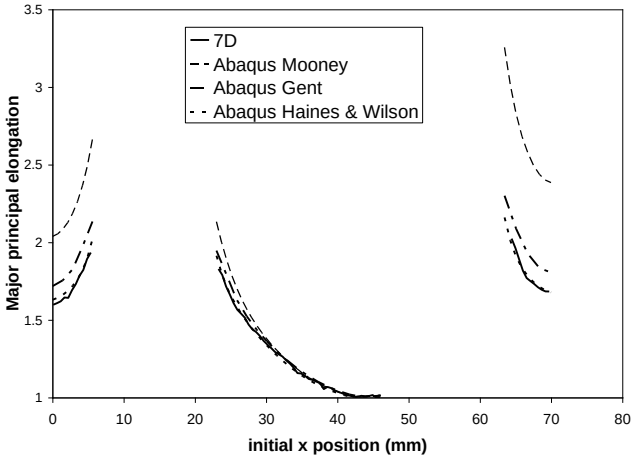

Figure 17. Experimental and simulated elongations along the lower path at 40N

Note that Haines & Wilson requires 6 parameters that allow it to fit to almost any hyperelastic experimental curve but it can also introduce numerical problems during calculation (Heuillet & Dugautier 1997). On the contrary, Gent needs only two parameters and still describes the silicone rubber quite well.

6 CONCLUSION

This paper first gives hints on how to model an unfilled silicone rubber but it also tests constitutive equations in a heterogeneous strain case. In particular, the study developed here shows the local errors made when using an inadequate model. The use of Mooney model for a material presenting an important strain hardening can lead to large overestimations of deformations for a given load. The use of the local strain field given by finite element analysis must be very carefully considered. This strain field is often used for crack tip analysis but errors can be very important. This emphasizes the uniaxial fit quality importance and the knowledge of the modelling limits.

ACKNOWLEDGEMENTS

L. Meunier thanks the Région Rhône-Alpes (France) for its financial support.

REFERENCES:

Boyce, M.C. 1996. Direct comparison of the Gent and the Arruda-Boyce constitutive models of rubber elasticity. *Rubber Chemistry and Technologies* 69: 781-785

Gent, A.N. 1996. A new constitutive relation for rubber. *Rubber Chemistry and Technologies* 69: 59-61

Goulbourne, N.C., Mockensturm, E.M., Frecker, M.I. 2007. Electro-elastomers: Large deformation analysis of silicone membranes. *International Journal of Solids and Structures* 44: 2609-2626.

Haines, D.W., Wilson, D.W. 1979. Strain energy density functions for rubber like materials. *Journal of the Mechanics and Physics of Solids* 27: 345-360.

Heulliet, P., Dugautier, L. 1997 Modélisation du comportement hyperélastique des élastomères compacts. *Génie Mécanique des caoutchoucs et des élastomères thermoplastiques, In Apollor Inpl LRCCP Firtech edition,* 67-103.

Loew, R., Meier P. 2006. Simulation of reiterated mechanical load of silicone rubber. *Finite Elements in Analysis and Design*,43: 453-462

Mooney, M. 1949. A theory of large elastic deformation. *Journal of Applied Physics* 11: 582-592.

Podnos, E., Becker E., Klawitter J., Strzepa, P. 2006. FEA analysis of silicone MCP implant. *Journal of Biomechanics* 39: 1217-1226.

Rivlin, E., Saunders, D.W. 1951. Large elastic deformations of isotropic materials- VII Experiments on the deformation rubber. *Philosophical Transactions of the Royal Society of London series A* 243: 251-288.

Vacher, P. 2003. Apport des techniques de corrélation d'images en mécanique : Analyse de déformations et numérisations 3D, Habilitation à diriger des recherches, Université de Savoie